Research Square

Preprints are preliminary reports that have not undergone peer review.
They should not be considered conclusive, used to inform clinical practice,
or referenced by the media as validated information.

Modeling Entanglement Purification in Leo Satellite Environment

Yifan Gao

yifan.gao@vuw.ac.nz

Victoria University of Wellington

Alvin Valera

Victoria University of Wellington

Wuyungerile Li

Inner Mongolia University

Winston Seah

Victoria University of Wellington

Research Article

Keywords: LEO Satellite, Classical Communication, Pumping Purification

Posted Date: November 24th, 2026

DOI: https://doi.org/10.21203/rs.3.rs-11836537/v1

License: This work is licensed under a Creative Commons Attribution 4.0 International License.
Read Full License

Additional Declarations: The authors declare no competing interests.

MODELING ENTANGLEMENT PURIFICATION IN LEO SATELLITE ENVIRONMENT

Yifan Gao[1] *Alvin Valera*[1] *Wuyungerile Li*[2] *Winston K.G. Seah*[1]

[1]School of Engineering and Computer Science, Victoria University of Wellington, New Zealand
[2]College of Computer Science, Inner Mongolia University, Hohhot, China

ABSTRACT

Pumping entanglement purification is commonly expected to increase fidelity toward one, an expectation that holds under idealized fiber-link assumptions. However, this convergence may fail in free-space inter-satellite links (ISLs), where classical communication delay is non-negligible and auxiliary Einstein-Podolsky-Rosen (EPR) pairs are generated over the same lossy channel as the retained pair. We analytically model pumping purification over a one-hop free-space ISL and characterize its attainable fidelity under these constraints. We derive a closed-form upper bound and prove that a failed purification round drives the retained EPR pair below the 0.5 fidelity threshold, preventing further purification. We further identify a critical distance of 46.76 km, beyond which purification provides no fidelity improvement in the considered 40–50 km range.

***Index Terms*—** LEO Satellite, Classical Communication, Pumping Purification

1. INTRODUCTION

Entanglement purification is done to raise fidelity without an intrinsic upper bound based on two assumptions that hold in fiber links, viz., the classical communication (CC) delay is negligible compared to the memory coherence time and each auxiliary pair is prepared at the fidelity of the target pair [1]. A free-space ISL violates both. The target Einstein-Podolsky-Rosen (EPR) pair decoheres while each auxiliary EPR pair is generated and heralded, and all EPR pairs are distributed over the same channel, so the fidelity of the auxiliary EPR pair never increases. The gain per purification therefore shrinks toward 0 while the waiting decoherence remains and fidelity converges not to 1 but to a bound set by the link distance.

Given two Low Earth Orbit (LEO) satellites connected by a single ISL, each equipped with a homogeneous quantum repeater of four-qubit capacity, with entanglement distributed over a noisy free-space channel and stored in quantum memories subject to amplitude damping, we **determine** the maximum fidelity attainable by repeated purification of a retained target EPR pair, to **optimize** the fidelity of the retained EPR pair over the number of purification rounds. This is subject to the **constraints** of the limited node capacity and the limited cutoff time of the quantum memories, the noisy free-space environment, the CC delay incurred in every round and the unheralded error of the local Controlled NOT (CNOT) gates.

We develop a mathematical model of entanglement pumping purification on a LEO ISL. One round is expressed as a 2×2 transfer matrix, so that k rounds are its k-th power and the analysis reduces to a steady state. We show that this steady state is a fidelity upper bound in closed form and that a failed purification leaves the retained EPR pair at a fidelity < 0.5, and it cannot be purified further. In addition, purification achieves no gain beyond 46.76 km.

2. BACKGROUND

Current models for entanglement purification are developed for fiber networks that either ignore the CC delay or treat it as a fixed overhead that does not enter the fidelity accounting [2, 3, 4]. A few models consider finite CC delay, but not together with a free-space channel and finite node capacity, and none examines whether repeated purification converges to a link-imposed limit. [1, 5, 6, 7].

We denote an EPR pair by $|\Phi^+\rangle = \frac{|00\rangle+|11\rangle}{\sqrt{2}}$ and its measured fidelity as $F = \langle\Phi^+|\rho|\Phi^+\rangle \in [0,1]$ where ρ is the actual density matrix. A noisy EPR pair is modelled by the Werner state $\rho(F) = F\ |\Phi^+\rangle\langle\Phi^+|\ + \frac{1-F}{3}(|\Phi^-\rangle\langle\Phi^-| + |\Psi^+\rangle\langle\Psi^+|\ +\ |\Psi^-\rangle\langle\Psi^-|)$ with $|\Phi^\pm\rangle = \frac{|00\rangle\pm|11\rangle}{\sqrt{2}}$ and $|\Psi^\pm\rangle = \frac{|01\rangle\pm|10\rangle}{\sqrt{2}}$. As it is Bell diagonal, the remaining probability $1 - F$ is distributed equally over the three orthogonal Bell states, each labeled by one error indicator $(i, j) \in \{0, 1\}^2$ where i indicates a bit-flip error and j indicates a phase-flip error. The pair carries usable entanglement only for $F > \frac{1}{2}$. Over an ISL, the link initial fidelity is set by Gaussian beam diffraction, the pointing error of the attitude control system, the polarization rotation of the acquisition (F_{rotation}), and pointing and tracking (APT) system, giving $F_0(d) = F_{\text{rotation}} \times \frac{\eta(d)+(1-\eta(d))\varepsilon}{1+3(1-\eta(d))\varepsilon}$, where $\eta(d)$ is the free-space transmittance [8], and ε is the Quantum Bit Error Rate (QBER) due to dark counts and background photons. Once stored, both qubits undergo amplitude damping independently, so a stored pair decays as $F(t) = F_0(d) \cdot e^{-2\Gamma t}$, where $\Gamma(s^{-1})$ is the amplitude damping rate and t. For a threshold F_{th}, any pair older than $K = \lfloor \frac{d}{c\Delta t} - \frac{1}{2\Gamma\Delta t} \ln \frac{F_{\text{th}}}{F_0} \rfloor$ slots is useless. Purification in

this paper follows the BBPSSW protocol [9], which uses local operations and classical communication (LOCC) to distill one EPR pair of higher fidelity from two EPR pairs of lower fidelity. That is, each satellite applies a local CNOT controlled by its target-pair qubit, measures the auxiliary qubit and exchanges the outcome via CC. Matching outcomes retain the target EPR pair, while differing outcomes discard both since the CNOT has already altered the target EPR pair irreversibly.

3. SYSTEM MODEL

This section discusses the LEO network scenario and purification procedure.

3.1. Scenario

We consider a single one-hop quantum link between two LEO satellites, source A and destination B, each having quantum memory of capacity four qubits. We assume the distance d is constant within the observation window, since the cutoff time of an entangled link is ≈ 0.3 s $\ll 5$ min, the contact window of inter-plane LEO satellites [8, 10]. Time is slotted with duration $\Delta t = 1$ ms and we write $\tau_{\text{cc}} = \left\lceil \frac{d}{c} + t_{\text{proc}}^{(\text{Classical})} \right\rceil \cdot \frac{1}{\Delta t} \geq 1$ for a one-way CC, where $t_{\text{proc}}^{(\text{Classical})}$ is the processing overhead. A link from A to B is established with probability $p' = p \cdot q_{\text{error}}(d) \cdot p_{\text{success}}(d)$, where p is the local generation probability at A, $q_{\text{error}}(d)$ is the probability that the photon is captured by B and $p_{\text{success}}(d)$ is the fidelity qualification rate. Each generation attempt takes $C(d) = \left\lceil \frac{1}{R_{\text{source}}} + \frac{d}{c} \right\rceil \cdot \frac{1}{\Delta t}$ time slots for generation and transmission, followed by a heralding interval of $\tau_{\text{herald}} = \tau_{\text{cc}}$ in which B reports the outcome. A full cycle requires $C(d) + \tau_{\text{herald}}$ slots and A knows each outcome before starting the next attempt. Purification has three kinds of timing overheads, throughout which the stored EPR pairs keep decohering. Firstly, the local CNOT and Bell-state measurement (BSM) on the auxiliary pair take τ_{gate} and τ_{BSM} slots. Secondly, a synchronization message $\tau_{\text{sync}} = \tau_{\text{cc}}$ precedes each jointly initiated action, so that both satellites act in the same slot. Lastly, a round-trip ACKnowledgement of $\tau_{\text{ack}} = 2\tau_{\text{cc}}$ slots returns the BSM outcomes m_A and m_B.

3.2. Purification timeline

We use E_1 to denote the target EPR pair, E_2 for the auxiliary EPR pair, $\mathcal{A}_i^{(t)}$ for the link age in slots of E_i, $i \in \{1, 2\}$, at instant t, counted from the instant the photon is captured and stored, so that $\mathcal{F}_i^{(t)} = F_0'(d) e^{-2\Gamma \mathcal{A}_i^{(t)} \Delta t}$. A single purification attempt proceeds as in Fig. 1. First, A generates E_1. Failed attempts consume time and qubits but leave no stored pair, so however many cycles it takes, E_1 is heralded at age τ_{herald}. E_2 then takes g further cycles, throughout which E_1 waits in memory, so at the instant t_2 at which E_2 is heralded, $\mathcal{A}_1^{(t_2)} = \tau_{\text{herald}} + g(C(d) + \tau_{\text{herald}}), \mathcal{A}_2^{(t_2)} = \tau_{\text{herald}}$. The two

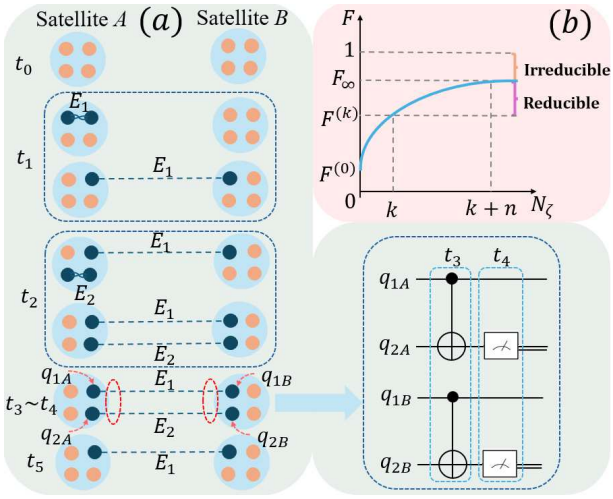


Fig. 1: (a) Purification Timeline and (b) Fidelity Gaps

EPR pairs therefore enter purification at different fidelities, where $\mathcal{F}_1^{(t_2)} < \mathcal{F}_2^{(t_2)}$. A failed attempt on E_2 ages E_1 while contributing nothing itself. A synchronization message precedes the bilateral CNOT, applied at $t_3 = t_2 + \tau_{\text{sync}} + \tau_{\text{gate}}$ and admissible only if $\mathcal{A}_1^{(t_3)} \leq K(d)$. A second synchronization precedes the auxiliary measurement, which ends at $t_4 = t_3 + \tau_{\text{sync}} + \tau_{\text{BSM}}$. The age of E_2 is frozen at the start of the readout window, at $\mathcal{A}_2^{(t_4 - \tau_{\text{BSM}})} = \tau_{\text{herald}} + 2\tau_{\text{sync}} + \tau_{\text{gate}}$ and E_2 is consumed at t_4. E_1 is not measured and decoheres through the readout, reaching $\mathcal{A}_1^{(t_4)} = \mathcal{A}_1^{(t_2)} + 2\tau_{\text{sync}} + \tau_{\text{gate}} + \tau_{\text{BSM}}$. The outcomes are then exchanged, so $t_5 = t_4 + \tau_{\text{ack}}$. The state of E_1 branches at t_4, not at t_5, the ACK carries only classical information and E_1 decoheres in both branches during $[t_4, t_5]$. With probability p_s the outcomes match and E_1 survives with $\mathcal{F}_1^{(t_5)} = F_{\text{post}}\, e^{-2\Gamma \tau_{\text{ack}} \Delta t}$, otherwise, both pairs are discarded and the process restarts, so the evolution of E_1 during that ACK does not enter any performance metric.

3.3. Bilateral CNOT

The bilateral CNOT is $U = CNOT_{q_{1A} \to q_{2A}} \otimes CNOT_{q_{1B} \to q_{2B}}$, acting in the computational basis as $U|a, b, c, d\rangle = |a, b, c \oplus a, d \oplus b\rangle$. The values of E_1 are unchanged while those of E_2 are combined with them, so that measuring E_2 reveals information about E_1 without measuring E_1. By the standard Pauli-propagation identities of the CNOT gate, a bit flip on the control propagates forward onto the gate target while a phase flip on the gate target is kicked back onto the control. Since E_1 supplies the controls and E_2 supplies the targets at both satellites, the error indicators transform as $E_1 \to (i_1, j_1 \oplus j_2)$ and $E_2 \to (i_1 \oplus i_2, j_2)$. The parity of the joint outcome therefore identifies the class of E_2 after U, since $m_A \oplus m_B = i_1 \oplus i_2$. A Φ-class state is supported on $|00\rangle$ and $|11\rangle$, so the two BSMs always agree. A Ψ-class state is supported on $|01\rangle$ and $|10\rangle$, so they always disagree. The

success condition $m_A = m_B$ is thus equivalent to $i_1 = i_2$, that is, the two pairs share the same bit-flip class. Defining $\Pi_{\text{succ}} = I_{q_{1A}q_{1B}} \otimes (|00\rangle\langle 00| + |11\rangle\langle 11|)_{q_{2A}q_{2B}}, \Pi_{\text{fail}} = I - \Pi_{\text{succ}}$ and writing $\rho_{\text{total}} = U(\rho_1 \otimes \rho_2)U^\dagger$ for the four-qubit state entering BSMs, the state of E_1 conditioned on success is $\sigma_{\text{succ}} = \frac{\text{Tr}_{q_{2A}q_{2B}}[\Pi_{\text{succ}}\rho_{\text{total}}\Pi_{\text{succ}}]}{p_s}$ and the post-purification fidelity is $F_{\text{post}} = \langle\Phi^+|\sigma_{\text{succ}}|\Phi^+\rangle$.

3.4. Success probability and post-purification fidelity

Summing the joint probabilities of the eight input combinations that leave E_2 in the Φ-class gives $p_s(F_1, F_2) = \frac{1}{9}(8F_1F_2 - 2F_1 - 2F_2 + 5)$. As σ_{succ} is Bell diagonal, F_{post} is its $|\Phi^+\rangle$ weight, which $i_1 = i_2$ together with $i_1 = 0$ and $j_1 \oplus j_2 = 0$ restricts to the inputs $|\Phi^+\rangle|\Phi^+\rangle$ and $|\Phi^-\rangle|\Phi^-\rangle$, whose phase flips cancel, so

$$F_{\text{post}}(F_1, F_2) = \frac{F_1F_2 + \frac{(1-F_1)(1-F_2)}{9}}{p_s(F_1, F_2)}.$$

The same construction applied to σ_{fail} admits only $|\Phi^+\rangle|\Psi^+\rangle$ and $|\Phi^-\rangle|\Psi^-\rangle$, giving $F_{\text{fail}}(F_1, F_2) < \frac{1}{2}$, whose numerator is the first of two products that are positive for $F_1, F_2 \in (0, 1)$. A failed round therefore ends the sequence rather than degrading it.

Gate errors are unheralded and the CNOT is self-inverse, so we model a faulty gate as noise, each satellite is ideal with probability $p_g \in (0, 1]$ and otherwise maximally mixes its two local qubits, leaving the parity bit uniform and the retained pair at fidelity $\frac{1}{4}$. Weighting that branch by $1 - p_g^2$ gives:

$$p_{s,\text{ng}}(F_1, F_2) = p_g^2 p_s(F_1, F_2) + \frac{1 - p_g^2}{2}$$

$$F_{\text{post,ng}}(F_1, F_2) = \frac{p_g^2\left[F_1F_2 + \frac{(1-F_1)(1-F_2)}{9}\right] + \frac{1-p_g^2}{8}}{p_{s,\text{ng}}(F_1, F_2)}$$

where $p_{s,\text{ng}}(F_1, F_2)$ and $F_{\text{post,ng}}(F_1, F_2)$ are the success probability and the post-fidelity of purification with noisy CNOT.

3.5. Decoherence factors

There are two intervals of decoherence in every purification round. Once E_1 has been heralded, it ages further, up to the projection instant, by $w = g(C(d) + \tau_{\text{herald}}) + 2\tau_{\text{syn}} + \tau_{\text{gate}} \ll K(d)$, which contains the E_2 generation, the two synchronization and the CNOT gate; it is also constrained by the cutoff K. Then, we have

$$\alpha = e^{-2\Gamma w\Delta t} \text{ and } \beta = e^{-2\Gamma(\tau_{\text{BSM}} + \tau_{\text{ack}})\Delta t}$$

where α is for the docoherence borne by E_1 before the projection and β is for the decoherence after it. The fidelities of E_1 and E_2 enter purification for a single round are

$$F_1 = F_0'(d)e^{-2\Gamma(\tau_{\text{herald}} + w)\Delta t}$$
$$F_2 = F_0'(d)e^{-2\Gamma(\tau_{\text{herald}} + 2\tau_{\text{sync}} + \tau_{\text{gate}})\Delta t}.$$

4. FIDELITY UPPER BOUND

At node capacity 4, each satellite holds one E_1 and one E_2 at a time.

4.1. Pumping recursion

Let $F^{(k)}$ denote the fidelity of E_1 after k successful rounds, evaluated at the instant t_5 at which the k-th ACK is confirmed, so that $F^{(k)}$ is both the output of round k and the input of round $k+1$. Round $k+1$ follows the timeline, except that E_1 is the survivor of round k rather than a fresh pair, so it waits for E_2 and enters the BSM at $\alpha F^{(k)}$. Each E_2 is freshly generated over the same channel and therefore enters at the same F_2 in every round and E_1 decoheres by β through the readout and the ACK. Hence $F^{(k+1)} = \beta F_{\text{post,ng}}(\alpha F^{(k)}, F_2) = G(F^{(k)})$, with $F^{(0)} = F_0'(d)e^{-2\Gamma\tau_{\text{herald}}\Delta t}$. The map G is linear fractional, $G(F) = \frac{m_{11}F + m_{12}}{m_{21}F + m_{22}}$, so one round is the matrix

$$M = \begin{pmatrix} m_{11} & m_{12} \\ m_{21} & m_{22} \end{pmatrix}, \begin{cases} m_{11} = 8\beta\alpha p_g^2(10F_2 - 1) \\ m_{12} = \beta(9 - p_g^2 - 8F_2p_g^2) \\ m_{21} = 16\alpha p_g^2(4F_2 - 1) \\ m_{22} = 4(p_g^2 - 4p_g^2F_2 + 9) \end{cases} \quad (1)$$

acting as $\left(F^{(k+1)}, 1\right)^\top \propto M\left(F^{(k)}, 1\right)^\top$ and k rounds are represented by M^k.

4.2. Steady state

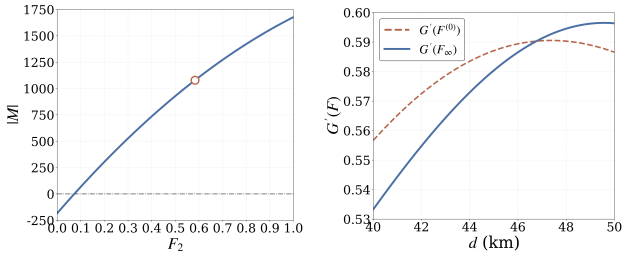
The fidelity attained after many purification rounds is $F_\infty = G(F_\infty)$ and $AF_\infty^2 + BF_\infty + C = 0$, where $A = m_{21}, B = m_{22} - m_{11}, C = -m_{12}$. The only one positive root of this function is

$$F_\infty(d) = \frac{-B + \sqrt{B^2 - 4AC}}{2A} \quad (2)$$

and the derivative of G is

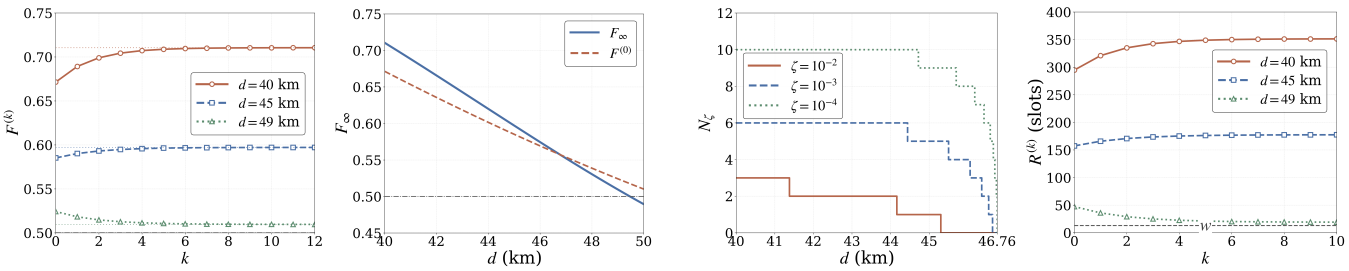
$$G'(F) = \frac{m_{11}m_{22} - m_{12}m_{21}}{(m_{21}F + m_{22})^2} = \frac{|M|}{(m_{21}F + m_{22})^2} \quad (3)$$

So, the map is increasing when $|M| = -48\alpha\beta p_g^2[16p_g^2F_2^2 - (8p_g^2 + 48)F_2 + (p_g^2 + 3)] > 0$, where $F_2 \geq 0.1$ is shown in Fig. 2(a) (the red circle is the F_2 in LEO scenario [8]), which



(a) $F_2 > 0.1 \Rightarrow \det M > 0 \Rightarrow G \uparrow$ (b) $G'(F) < 1 \Rightarrow G$ convergences

Fig. 2: Monotonicity and Convergence Rate of Pumping Map



(a) $F^{(k)}$ converging to F_∞ (b) F_∞ and $F^{(0)}$ crossing at 46.76 km (c) Purification end index N_ζ (d) Residual Lifetime of E_1

Fig. 3: Pumping Convergence over ISL $d \in [40, 49]$ km

means G is increasing monotonously when $F_2 \in [0.1, 1]$, so every purification round moves the fidelity toward $F_\infty(d)$ and never past it.

Let $e_k = F_\infty - F^{(k)}$ be the gap left after k rounds. Perform a first-order Taylor expansion near the fixed point F_∞, one more round moves $F^{(k)}$ to $G(F^{(k)})$ while F_∞ stays fixed, so $e_{k+1} = G(F_\infty) - G(F^{(k)})$ and over a small gap G is well approximated by its tangent at F_∞ as $e_{k+1} \simeq \lambda e_k, \lambda = G'(F_\infty) = \frac{|M|}{(AF_\infty + m_{22})^2}$. Each round shrinks the gap by the same factor, so after k rounds it is roughly λ^k times its initial value. Fig. 2(b) gives $\lambda \in (0.53, 0.6)$ over $d \in [40, 50]$ km, close to 0 means the bound is reached in a few rounds, close to 1 means many rounds are needed.

We separate the remaining infidelity after k rounds into the part that pumping cannot overcome and the part that can be overcome by more rounds as $1 - F^{(k)} = [1 - F_\infty] + [F_\infty - F^{(k)}]$ (as illustrated in Fig. 1(b)) [11]. The first term is set by the free-space channel through F_2 and by the waiting decoherence through α, and it is the gap from F_∞ to 1 that cannot be reduced. Only the second term can decrease with the depth of the purification protocol, which is therefore the term that determines how long pumping is worth continuing. The minimum number of rounds once the second term is lower than the tolerance ζ follows $\lambda^k |F_\infty - F^{(0)}| \leq \zeta$, then dividing by $\ln \lambda$, which is negative because $\lambda < 1$ and therefore the minimum pumping end index is:

$$N_\zeta \simeq \left\lceil \frac{\ln \frac{\zeta}{|F_\infty - F^{(0)}|}}{\ln \lambda} \right\rceil . \tag{4}$$

Meanwhile, a purification round is admissible only if E_1 is still well entangled at the projection instant. An EPR pair held at fidelity F decays as $Fe^{-2\Gamma t}$, so the residual time it stays alive in quantum memories before it reaches the useless fidelity threshold of $F_{\text{th}} = \frac{1}{2}$ at the k-th purification round is:

$$R^{(k)} = \frac{1}{2\Gamma \Delta t} \ln 2F^{(k)} \tag{5}$$

and round $k+1$ is admissible when $w \leq R^{(k)}$.

5. EVALUATION

We evaluate the model over $d \in [40, 50]$ km, with $\Gamma = 0.5\ s^{-1}, p_g = 0.99, g = 5$ [8]. Fig. 3(a) shows the trend of $F^{(k)}$ approaching F_∞. At 40 km and 45 km, F_∞ rises monotonically to its bound, from 0.67 to 0.71 and from 0.59 to 0.60, settling in about six rounds. However, at 49 km, it falls from 0.52 to 0.51, and while the recursion still converges, it goes below its starting point. Fig. 3(b) explains this. Both $F^{(0)}(d)$ and $F_\infty(d)$ decrease with d but $F_\infty(d)$ decreases faster and they cross at $d = 46.76$ km, which is therefore the maximum distance where pumping is effective. Every round can only raise F_1 for $d \in [40, 46]$ km. Fig. 3(c) shows the minimum number of rounds needed to bring $F^{(k)}$ to its F_∞. At $\zeta = 10^{-3}$, it falls in discreet steps from 6 rounds at 40 km to 4 at 46 km. This is not caused by faster convergence, that $G'(F_\infty)$ actually grows from 0.53 to 0.60 over $d \in [40, 50]$ km (Fig. 2(b)), but the initial gap $|F_\infty - F^{(0)}|$ shrinks as the crossing is approached. Fig. 3(d) shows that with $w = 13$ slots, $R^{(k)}$ grows from 295 to 351 slots at 40 km and from 157 to 178 slots at 45 km and even at 49 km, where pumping degrades the pair as $R^{(k)}$ shrinks from 47 to 19 slots, it still ends up 6 slots more than w. Purification is thus limited by whether a round yields a gain, not by memory lifetime.

6. CONCLUSION

This paper models entanglement pumping purification over a one-hop free-space LEO link and shows that the fidelity it can attain is bounded by decoherence during the waiting time. We describe one purification round as a 2×2 transfer matrix acting on the fidelity of the retained EPR pair and so the fidelity after k rounds is the k-th power of that matrix. We also proved that a failed purification round leaves the fidelity of the retained EPR pair below $1/2$ and can not be restored by further purification. Moreover, we find that over the ISL distance of 40 to 46 km, the fidelity upper bound can be reached within 10 rounds at a tolerance of 10^{-4} and purification gives no gain beyond 46.76 km. Therefore, designing a strategy to overcome this bound is our future work.

7. ACKNOWLEDGMENTS

The work of Yifan Gao was supported by the China Scholarship Council (CSC), Grant No. 202508250019.

8. REFERENCES

[1] Vivek Vasan, Alexander Nico-Katz, Boulat A Bash, Daniel C Kilper, and Marco Ruffini, "Entanglement Purification With Finite Latency Classical Communication in Quantum Networks," *arXiv preprint:2509.03667*, 2025.

[2] Nitish K Panigrahy, Thirupathaiah Vasantam, Don Towsley, and Leandros Tassiulas, "On the Capacity Region of a Quantum Switch With Entanglement Purification," in *INFOCOM Conference on Computer Communications*. IEEE, 2023, pp. 1–10.

[3] Jiyao Liu, Xinwen Zhang, Xinliang Wei, Xuanzhang Liu, Yuzhou Chen, Hongchang Gao, and Yu Wang, "Joint Swapping and Purification With Failures for Entanglement Distribution in Quantum Networks," in *ACM 33rd International Symposium on Quality of Service (IWQoS)*. IEEE, 2025, pp. 1–10.

[4] Allen Zang, Xin-An Chen, Eric Chitambar, Martin Suchara, and Tian Zhong, "Entanglement Purification in Quantum Networks: Guaranteed Improvement and Optimal Time," *arXiv preprint:2505.02286*, 2025.

[5] Michelle Victora, Spyros Tserkis, Stefan Krastanov, Alexander Sanchez de la Cerda, Steven Willis, and Prineha Narang, "Entanglement Purification on Quantum Networks," *Physical Review Research*, vol. 5, no. 3, pp. 033171, 2023.

[6] Anoosha Fayyaz, Prashant Krishnamurthy, Kaushik Seshadreesan, Amy Babay, and David Tipper, "To Purify or Not to Purify: Entanglement Purification under Input Fidelity Asymmetry in Quantum Networks," *arXiv preprint:2605.08771*, 2026.

[7] Wenhan Li and Shiyu Zhang, "Simulation of Quantum Repeater Networks under Decoherence and Purification Constraints," *arXiv preprint:2510.07471*, 2025.

[8] Yifan Gao, Alvin Valera, and Winston K. G. Seah, "Markov Chain Model of Entanglement Setup in Noisy Dynamic LEO Satellite Networks," *arXiv preprint:2512.20047*, 2025.

[9] Charles H Bennett, Gilles Brassard, Sandu Popescu, Benjamin Schumacher, John A Smolin, and William K Wootters, "Purification of Noisy Entanglement and Faithful Teleportation via Noisy Channels," *Physical review letters*, vol. 76, no. 5, pp. 722, 1996.

[10] Arman Mollakhani, Jerayu Tiamraj, Shu-Jie Cao, and Dongning Guo, "Inter-Satellite Link Configuration for Fast Delivery in Low-Earth-Orbit Constellations," in *Aerospace Conference*. IEEE, 2026, pp. 1–9.

[11] Yuta Kikuchi, Conor Mc Keever, Luuk Coopmans, Michael Lubasch, and Marcello Benedetti, "Realization of Quantum Signal Processing on a Noisy Quantum Computer," *npj Quantum Information*, vol. 9, no. 1, pp. 93, 2023.